Title

Whole knee joint mapping using a phase modulated UTE adiabatic T1ρ (PM-UTE-AdiabT1ρ) sequence

Journal

Magnetic Resonance in Medicine, 91(3)

ISSN

0740-3194

Authors

Ma, Yajun

Carl, Michael

Tang, Qingbo

et al.

Publication Date

2024-03-01

DOI

10.1002/mrm.29871

Peer reviewed

HHS Public Access

Author manuscript

Magn Reson Med. Author manuscript; available in PMC 2024 March 01.

Published in final edited form as:

Magn Reson Med. 2024 March ; 91(3): 896–910. doi:10.1002/mrm.29871.

Whole Knee Joint Mapping Using a Phase Modulated Ultrashort Echo Time Adiabatic $T_{1\rho}$ (PM-UTE-Adiab$T_{1\rho}$) Sequence

Yajun Ma[1], **Michael Carl**[2], **Qingbo Tang**[1,3], **Dina Moazamian**[1], **Jiyo S Athertya**[1], **Hyungseok Jang**[1], **Susan V Bukata**[4], **Christine B Chung**[1,3], **Eric Y Chang**[1,3], **Jiang Du**[1,3,5]

[1]Department of Radiology, University of California San Diego, CA, USA

[2]GE Healthcare, San Diego, CA, USA

[3]Radiology Service, Veterans Affairs San Diego Healthcare System, CA, USA

[4]Department of Orthopaedic Surgery, University of California San Diego, CA, USA

[5]Department of Bioengineering, University of California San Diego, CA, USA

Abstract

Purpose: To develop a 3D phase modulated ultrashort echo time adiabatic $T_{1\rho}$ (PM-UTE-Adiab$T_{1\rho}$) sequence for whole knee joint mapping on a clinical 3T scanner.

Methods: This new sequence includes six major features: 1) a magnetization reset module, 2) a train of adiabatic full passage pulses for spin locking, 3) a phase modulation scheme (i.e., RF cycling pair), 4) a fat saturation module, 5) a variable flip angle scheme, and 6) a 3D UTE Cones sequence for data acquisition. A simple exponential fitting was used for $T_{1\rho}$ quantification. Phantom studies were performed to investigate PM-UTE-Adiab$T_{1\rho}$'s sensitivity to compositional changes and reproducibility as well as its correlation with continuous-wave $T_{1\rho}$ (CW-$T_{1\rho}$) measurement. The PM-UTE-Adiab$T_{1\rho}$ technique was then applied to five ex vivo and five in vivo normal knees to measure $T_{1\rho}$ values of femoral cartilage, meniscus, posterior cruciate ligament (PCL), anterior cruciate ligament (ACL), patellar tendon, and muscle.

Results: The phantom study demonstrated PM-UTE-Adiab$T_{1\rho}$'s high sensitivity to compositional changes, its high reproducibility, and its strong linear correlation with CW-$T_{1\rho}$ measurement. The ex vivo and in vivo knee studies demonstrated average $T_{1\rho}$ values of 105.6±8.4 and 77.9±3.9ms for the femoral cartilage, 39.2±5.1 and 30.1±2.2ms for the meniscus, 51.6±5.3 and 29.2±2.4ms for the PCL, 79.0±9.3 and 52.0±3.1ms for the ACL, 19.8±4.5 and 17.0±1.8ms for the patellar tendon, and 91.1±8.8 and 57.6±2.8ms for the muscle, respectively.

Conclusion: The 3D PM-UTE-Adiab$T_{1\rho}$ sequence allows volumetric $T_{1\rho}$ assessment for both short and long T_2 tissues in the knee joint on a clinical 3T scanner.

Keywords

$T_{1\rho}$; Adiab$T_{1\rho}$; ultrashort echo time; whole knee imaging

Corresponding Author: Yajun Ma, Ph.D., yam013@ucsd.edu, Department of Radiology, University of California, San Diego, 9452 Medical Center Dr., San Diego, CA 92037, Phone (858) 246-2229, Fax (858) 246-2221.

Introduction

Spin lattice relaxation in the rotating frame ($T_{1\rho}$) has been proposed as an MR imaging biomarker of tissue degeneration in the musculoskeletal (MSK) system [1]. Many studies have shown that $T_{1\rho}$ is sensitive to compositional changes in cartilage, e.g., loss of proteoglycans (PGs), which can be potentially useful for early diagnosis of osteoarthritis (OA) [2–4].

However, the commonly used continuous wave type $T_{1\rho}$ (CW-$T_{1\rho}$) imaging on clinical MRI is subject to the magic angle effect which may affect the quantification of highly anisotropic tissues such as the articular cartilage, menisci, ligaments, and tendons [5–10]. The CW-$T_{1\rho}$ values may increase more than 100% when the tissue fibers reorientate from 0° to 55° relative to the B_0 field [6–8]. These magic angle-induced CW-$T_{1\rho}$ changes may be much greater than those induced by tissue degeneration, making the clinical assessment of tissue pathological changes complicated.

Recently, a new strategy using a train of adiabatic full passage (AFP) pulses for spin locking was proposed to produce $T_{1\rho}$ contrast (i.e., Adiab$T_{1\rho}$) [10–12]. Adiab$T_{1\rho}$ is able to detect degenerative and biomechanical changes in cartilage and tendons [13–17]. These new Adiab$T_{1\rho}$ sequences have two major advantages over the conventional CW-$T_{1\rho}$ sequences. The first advantage is that the measured $T_{1\rho}$ from the Adiab$T_{1\rho}$ sequence is much less sensitive to the magic angle effect than that measured from the CW-$T_{1\rho}$ sequence at 500 Hz on a clinical MRI scanner, as shown in both cartilage and tendon studies [8,9]. The second advantage is that the Adiab$T_{1\rho}$ imaging is insensitive to B_1 inhomogeneity because of the use of adiabatic pulses for spin locking [11]. In contrast, the conventional CW-$T_{1\rho}$ imaging suffers banding artifacts related to B_1 inhomogeneity [18–20].

Most recently, we have combined a 3D ultrashort echo time sequence with the Adiab$T_{1\rho}$ preparation (UTE-Adiab$T_{1\rho}$) for volumetric $T_{1\rho}$ imaging [17,21]. This UTE-Adiab$T_{1\rho}$ sequence allows a comprehensive assessment of all the major tissue components in the knee joint, including both short (e.g., the deep radial and calcified cartilage, menisci, ligaments, and tendons) and long T_2 (e.g., the middle and superficial cartilage, and muscles) tissues and tissue components [21,22]. However, the tissue T_1 value should be estimated for accurate $T_{1\rho}$ quantification in this sequence, as can be seen in Eq. [1] in Ref. [21]. This T_1 measurement increases the total scan time, and errors in T_1 quantification lead to inaccurate $T_{1\rho}$ quantification.

In this study, inspired by the widely used 3D magnetization-prepared angle-modulated partitioned k-space spoiled gradient echo snapshots (MAPSS) sequence [23], we developed a new UTE-Adiab$T_{1\rho}$ framework, i.e., a phase-modulated UTE adiabatic $T_{1\rho}$ (PM-UTE-Adiab$T_{1\rho}$) sequence, for quantitative $T_{1\rho}$ imaging of all major tissue components in the knee joint. With this new PM-UTE-Adiab$T_{1\rho}$ sequence, $T_{1\rho}$ is estimated using a simple exponential fitting model, and T_1 information is no longer needed for accurate $T_{1\rho}$ quantification. To investigate the accuracy of this new PM-UTE-AdiabT1rho sequence, phantoms with different agarose concentrations were made and scanned on a 3T clinical MRI scanner. Phantoms with different agarose concentrations and $MnCl_2$ concentrations (i.e., with different T_1 relaxation times) were also scanned to investigate potential T_1

contamination caused by the usage of AFP pulses with relatively long durations for spin locking, a concern raised by Pang Y in a recent letter article [24]. Finally, the new sequence was applied to five ex vivo human knee joint specimens and five in vivo knee joints of healthy volunteers for $T_{1\rho}$ measurements for the femoral cartilage, meniscus, posterior cruciate ligament (PCL), anterior cruciate ligament (ACL), patellar tendon, and muscle.

Methods

Sequence and Signal Model

Figure 1 shows the diagram of the proposed PM-UTE-Adiab$T_{1\rho}$ sequence. This new sequence includes six major features: 1) a magnetization reset module to produce a consistent magnetization recovery [23], 2) a train of AFP pulses to produce $T_{1\rho}$ contrast [21], 3) a phase modulation scheme (i.e., RF cycling scheme using a 90° pulse pair) to mitigate the influence of T_1 dependence during the signal evolution within the data acquisition period [23], 4) a fat saturation module between the $T_{1\rho}$ preparation and acquisition blocks for fat suppression, 5) a variable flip angle (VFA) scheme to reduce signal variation along the multiple data acquisition spokes [23], and 6) a 3D UTE sequence for data acquisition with an efficient Cones encoding trajectory and a minimal nominal echo time (TE) of 32 μs (pulse duration is not included in the nominal TE calculation) [25].

The RF cycling strategy (i.e., the third feature) is applied to adjacent acquisitions with the same gradient encodings [23]. During the second acquisition, the phase of the second 90° pulse in the RF cycling pair alternates 180°. The two acquisitions are interleaved. The final image is reconstructed from the subtracted data between these adjacent acquisitions with opposite cycling phases. The magnetization reset, phase modulation, and VFA design features have been successfully applied to the 3D MAPSS sequence [23].

The transverse signal after the i^{th} ($i = 1, 2, 3, \ldots, N_{sp}$, N_{sp} is the total number of excitations or spokes in each TR) excitation in the n^{th} TR is expressed as follows:

$$M_{xy}(i) = a(i)M_{prep} + b(i) \quad [1]$$

where $a(i) = e^{-t_0/T_1}e_1^{i-1}[\prod_{j=1}^{i-1}\cos(\alpha_j)]e_2\sin(\alpha_i)$

$$b(i) = M_0\left(1 - e^{-t_0/T_1}\right)\{\sum_{p=1}^{i}[e_1^{i-p}\prod_{j=p}^{i-1}\cos(\alpha_j)]\}e_2\sin(\alpha_i)$$

$$e_1 = e^{-\tau/T_1} \text{ and } e_2 = e^{-TE/T_2^*}$$

α_i is the flip angle (FA) of i^{th} excitation. M_{prep} represents the longitudinal signal at the end of the RF cycling pair, and t_0 is the time gap between the RF cycling pair and the signal

acquisition segment. τ is the time interval between adjacent excitations or spokes. $a(i)$ and $b(i)$ are terms related to tissue T_1.

In the next TR (i.e., (n+1)th TR), the phase of the second 90° pulse in the RF cycling pair alternates by 180°. Thus, the longitudinal signal at the end of the RF cycling pair becomes $-M_{prep}$. The transverse signal after the i^{th} excitation in the (n+1)th TR is expressed as follows:

$$M_{xy}(i) = -a(i)M_{prep} + b(i) \quad [2]$$

After subtraction between signals acquired from the above two adjacent TRs (i.e., Eq. [1] – Eq. [2]), the signal equation becomes:

$$M_{xy}(i) = 2a(i)M_{prep} \quad [3]$$

The $T_{1\rho}$ independent term $b(i)$ is canceled. Since M_{prep} is proportional to the term of $e^{-TLS/T_{1\rho}}$ and $a(i)$ is independent of tissue $T_{1\rho}$, the subtracted signal $M_{xy}(i)$ is proportional to $e^{-TLS/T_{1\rho}}$. TSL is the spin locking time, determined by the multiplication of the total number of AFP pulses (N_{AFP}) and the AFP pulse duration.

As seen in Eq. [3], the signal intensities in different spokes are modulated by $a(i)$, which can produce signal variations and lead to image artifacts. To mitigate this signal variation, the VFA scheme is incorporated into the sequence, and the FA of i^{th} excitation (i.e., α_i) is determined according to the following equation:

$$a(i) = a(i+1) \quad [4]$$

which requires

$$\tan(\alpha_i) = e_1 \sin(\alpha_{i+1}) \text{ or } \alpha_i = \text{atan}[e_1 \sin(\alpha_{i+1})] \quad [5]$$

Once the last FA (i.e., $\alpha_{N_{sp}}$) is determined, the FAs of the rest excitations in a TR can be easily calculated by Eq. [5]. Then the signals acquired among different spokes have identical intensities for a tissue.

To estimate $T_{1\rho}$, multiple data are acquired by the PM-UTE-AdiabT$_{1\rho}$ sequence with different TSLs (i.e., different numbers of AFP pulses) and fitted with a single exponential function [23]:

$$M_{xy} = Ae^{-TSL/T_{1\rho}} \quad [6]$$

where A is a constant term that is independent of $T_{1\rho}$.

Phantom Study

The PM-UTE-Adiab$T_{1\rho}$ sequence was implemented on a 3T clinical MRI scanner (GE Healthcare Technologies, Milwaukee, WI) and scanned with an 8-channel transmit/receive knee coil. An AFP pulse (hyperbolic secant type I pulse) with a duration of 6.048 ms, a bandwidth of 1.643 kHz, and a maximum B_1 amplitude of 17μT was used to generate $T_{1\rho}$ contrast in the PM-UTE-Adiab$T_{1\rho}$ sequence [26,27]. A rectangular pulse with a duration of 270 μs was used for UTE signal excitation.

To validate the accuracy of the developed PM-UTE-Adiab$T_{1\rho}$ sequence in $T_{1\rho}$ measurement, four phantoms were prepared with different agarose concentrations (1%, 2%, 3%, and 4%, weight/volume (w/v)) and scanned together with the following parameters: field of view (FOV) = 16×16 mm^2, matrix = 192×192, slice number = 30, slice thickness = 4 mm, spoke interval (τ)/TE = 4.2/0.032 ms, magnetization recovery time (T_{rec}) = 330 ms, TSL = 0, 12.1, 24.2, 36.3, 48.4, 72.6, and 96.9 ms, number of TRs = 182, duration of each TR = ~650 ms, total number of spokes = 11758, N_{sp} = 65, $\alpha_{N_{sp}} = 60°$, bandwidth = 125 kHz, acquisition window stretch factor = 1, and total scan time = ~14 min. Reproducibility of the PM-UTE-Adiab$T_{1\rho}$ sequence was investigated using these agarose phantoms by repeating the protocol two times and the MRI system was reset before each PM-UTE-Adiab$T_{1\rho}$ scan.

The phase modulation strategy employed in the proposed PM-UTE-Adiab$T_{1\rho}$ sequence was expected to minimize T_1 dependence during signal evolution in the data acquisition period. To investigate this issue, a PM-UTE-CW-$T_{1\rho}$ sequence was also implemented with an identical sequence structure as the proposed PM-UTE-Adiab$T_{1\rho}$ except the utilization of the CW-$T_{1\rho}$ preparation. The CW-$T_{1\rho}$ scheme in the PM-UTE-CW-$T_{1\rho}$ sequence was similar to that used in the MAPSS CW-$T_{1\rho}$ sequence [23]. Four series of phantoms with different agarose concentrations (1%, 2%, 3% and 4% w/v) were prepared to compare the $T_{1\rho}$ quantification between PM-UTE-CW-$T_{1\rho}$ and MAPSS CW-$T_{1\rho}$. In each series, four different phantoms were prepared with different $MnCl_2$ concentrations to change their T_1 relaxation times. Supplemental Information Table S1 shows more detailed information of these phantoms in terms of the agarose and $MnCl_2$ concentrations as well as their T_1 values as measured by a VFA technique with B_1 correction [28]. These phantoms were then scanned with 3D PM-UTE-CW-$T_{1\rho}$ and MAPSS CW-$T_{1\rho}$ sequences for comparison with following parameters: 1) PM-UTE-CW-$T_{1\rho}$: FOV = 14×14 mm^2, matrix = 192×192, slice number = 36, slice thickness = 4 mm, τ/TE = 4.2/0.032 ms, T_{rec} = 800 ms, spin lock frequency = 500 Hz, TSL = 0, 10, 30, and 60 ms, N_{sp} = 64, $\alpha_{N_{sp}} = 60°$, bandwidth = 125 kHz, and total scan time = ~17 min; 2) MAPSS CW-$T_{1\rho}$: FOV = 14×14 mm^2, matrix = 192×192, slice number = 36, slice thickness = 4 mm, τ/TE = 4.9/2.2 ms, T_{rec} = 800 ms, spin lock frequency = 500 Hz, TSL = 0, 10, 30, and 60 ms, N_{sp} = 64, $\alpha_{N_{sp}} = 90°$, bandwidth = 125 kHz, and total scan time = ~11 min.

Furthermore, to investigate the relationship of the $T_{1\rho}$ measurements between Adiab$T_{1\rho}$ and CW-$T_{1\rho}$, three series of phantoms with different agarose concentrations (1%, 2%, and 3% w/v) were prepared and scanned with both 3D PM-UTE-Adiab$T_{1\rho}$ and MAPSS CW-$T_{1\rho}$

sequences. In each series, four different phantoms were prepared with different $MnCl_2$ concentrations to change their T_1 relaxation times. Detailed information of these phantoms can be seen in Table 1. The sequence parameters of the PM-UTE-Adiab$T_{1\rho}$ were identical to those used in the first phantom study above except for the following parameters: FOV = 14×14 mm^2, slice number = 36 and slice thickness = 4 mm. The MAPSS CW-$T_{1\rho}$ sequence was scanned with identical sequence parameters used in the second phantom study.

Ex Vivo Knee Study

Five normal cadaveric knee joints from five donors (aged 38–87 years, mean age 55.6 years; 2 male, 3 females) were scanned by the PM-UTE-Adiab$T_{1\rho}$ sequence at room temperature using the following parameters: FOV = 15×15 mm^2, matrix = 256×256, slice number = 40, slice thickness = 2 mm, τ/TE = 6/0.032 ms, T_{rec} = 330 ms, TSL = 0, 12.1, 24.2, 36.3, 48.4, 72.6, and 96.9 ms, number of TRs = 316, duration of each TR = ~700 ms, total number of spokes = 20530, N_{sp} = 65, $\alpha_{N_{sp}} = 60°$, bandwidth = 125 kHz, acquisition window stretch factor = 1, and total scan time = ~25 min.

In Vivo Knee Study

Five normal knee joints from five volunteers (aged 34-40 years, mean age 37.5 years; 4 males, 1 female) were also scanned. Informed consent was obtained from all subjects in accordance with the guidelines of the institutional review board. The PM-UTE-Adiab$T_{1\rho}$ sequence was used to scan these knee joints with the following parameters: FOV = 15×15 mm^2, matrix = 256×256, slice number = 32, slice thickness = 3 mm, τ/TE = 5.5/0.032 ms, T_{rec} = 330 ms, TSL = 0, 12.1, 24.2, 36.3, 48.4, 72.6 and 96.9 ms, number of TRs = 150, duration of each TR = ~900 ms, total number of spokes = 11186, N_{sp} = 75, $\alpha_{N_{sp}} = 60°$, bandwidth = 125 kHz, acquisition window stretch factor = 1.5, and total scan time = ~16 min.

Data Analysis

Single exponential fitting was performed on the magnitude data, and the image background noise was estimated and incorporated as a constant term in the fitting process. The mean value of the background noise was calculated from a carefully selected 8×8 object-free region (avoiding regions with artifacts) on the PM-UTE-Adiab$T_{1\rho}$ image with the longest TSL. The data processing code was written in Matlab (The MathWorks Inc., Natick, MA, USA), and the Levenberg-Marquardt algorithm was used to solve the non-linear least-squares optimization problem [29,30]. The Intraclass Correlation Coefficient (ICC) analysis was used to evaluate the reproducibility of $T_{1\rho}$ measurement for the phantom study. Pearson correlation was used to investigate the correlations between PM-UTE-Adiab$T_{1\rho}$, MAPSS CW-$T_{1\rho}$ and T_1, and between PM-UTE-CW-$T_{1\rho}$ and MAPSS CW-$T_{1\rho}$ as well as between PM-UTE-Adiab$T_{1\rho}$ and MAPSS CW-$T_{1\rho}$. A P-value less than 0.05 is considered statistically significant. Regions of interest (ROIs) were manually drawn for various tissues, including the articular cartilage, meniscus, PCL, ACL, patellar tendon, and muscle in all knee joints. Mean $T_{1\rho}$ and standard deviation (STD) values for all the major tissue components in both ex vivo and in vivo knee joints were calculated.

Results

Figure 2 shows the results from the first phantom study. As can be seen in the $T_{1\rho}$ map in Figure 2b, the $T_{1\rho}$ values decrease with the higher agarose concentrations in the phantoms. Excellent linear correlation is achieved between $R_{1\rho}$ (=1/$T_{1\rho}$) values and agarose concentrations with an R^2 of 0.9999. The $T_{1\rho}$ map of the second scan (Figure 2d) shows similar $T_{1\rho}$ distributions to that of the first scan (Figure 2b). Two repeated scans show an excellent ICC (R^2 = 0.9996), demonstrating great reproducibility of the PM-UTE-Adiab$T_{1\rho}$ technique.

Supplemental Information Figure S1 shows the correlation curve between PM-UTE-CW-$T_{1\rho}$ MAPSS CW-$T_{1\rho}$ measurements for the twelve phantoms. T_1 values of these phantoms ranged from ~600 to ~1700 ms (see Supplemental Information Table S1), which cover the spectrum of T_1 values for all major tissues in the knee joint [28]. A very strong correlation was found between PM-UTE-Adiab$T_{1\rho}$ and MAPSS CW-$T_{1\rho}$ measures (R^2 = 0.9971, P < 0.0001). The obtained linear regression equation demonstrated a similar range of $T_{1\rho}$ measurements (i.e., [20, 100] ms) between these two techniques.

Figure 3 shows the T_1, PM-UTE-Adiab$T_{1\rho}$, and MAPSS CW-$T_{1\rho}$ mapping results from the second phantom study. This T_1 map displays a wide range of T_1 relaxation times from ~600 to ~1500 ms (T_1 values are shown in Table 1). The $T_{1\rho}$ values in the PM-UTE-Adiab$T_{1\rho}$ maps are generally higher than the corresponding MAPSS CW-$T_{1\rho}$ measurements. Notably, the $T_{1\rho}$ values of these phantoms demonstrate a similar visual trend for the two kinds of $T_{1\rho}$ measurement techniques. Figure 4 shows the correlation curves between MAPSS CW-$T_{1\rho}$, PM-UTE-Adiab$T_{1\rho}$ and T_1, and between PM-UTE-Adiab$T_{1\rho}$ and MAPSS CW-$T_{1\rho}$ for the twelve phantoms. A similar moderate correlation was found between MAPSS CW-$T_{1\rho}$ measures and T_1 values (R^2 = 0.3846, P = 0.031) and between PM-UTE-Adiab$T_{1\rho}$ measures and T_1 values (R^2 = 0.3633, P = 0.038), while a very strong correlation was found between PM-UTE-Adiab$T_{1\rho}$ and MAPSS CW-$T_{1\rho}$ measures (R^2 = 0.9985, P < 0.0001).

Figure 5 shows representative PM-UTE-Adiab$T_{1\rho}$ images acquired from a knee joint specimen (45-year-old male donor). Both long T_2 (e.g., the cartilage and muscle) and short T_2 tissue (e.g., the meniscus, quadriceps tendon, patellar tendon, ACL and PCL) signals are detected by the PM-UTE-Adiab$T_{1\rho}$ sequence. Fat signals are efficiently suppressed in all images at different TSLs. As can be seen in Figure 6, excellent single exponential fitting is achieved for the major knee tissue components including the femoral cartilage, meniscus, PCL, ACL, patellar tendon, and muscle, where the $T_{1\rho}$ values of these tissues are 90.3±10.1, 37.7±1.6, 46.8±1.1, 76.7±9.5, 13.4±0.6, and 74.8±5.8 ms, respectively.

Figure 7 shows representative PM-UTE-Adiab$T_{1\rho}$ images acquired from an in vivo knee joint (36-year-old female volunteer). Similar to the ex vivo knee study, both short and long T_2 tissue signals in the knee joint are well detected by this new sequence, while fat signals are efficiently suppressed. As can be seen in Figure 8, excellent single exponential fitting is achieved for all the major knee tissue components. The $T_{1\rho}$values of the femoral cartilage, meniscus, PCL, ACL, patellar tendon, and muscle are 73.2±2.6, 34.6±1.2, 30.0±0.8, 47.6±2.0, 15.6±0.3, and 61.2±3.2 ms, respectively.

Table 2 summarizes the $T_{1\rho}$ measurements for both ex vivo and in vivo knee joints. The average $T_{1\rho}$ values of femoral cartilage, meniscus, PCL, ACL, patellar tendon, and muscle for the five normal knee joint specimens are 105.6±8.4, 39.2±5.1, 51.6±5.3, 79.0±9.3, 19.8±4.5, and 91.1±8.8 ms, respectively. The average $T_{1\rho}$ values of the femoral cartilage, meniscus, PCL, ACL, patellar tendon, and muscle for the five normal in vivo knee joints are 77.9±3.9, 30.1±2.2, 29.2±2.4, 52.0±3.1, 17.0±1.8, and 57.6±2.8 ms, respectively. The ex vivo $T_{1\rho}$ measures are generally higher than the in vivo measurements because of the lower tissue temperature (room temperature vs. body temperature) and potential degeneration of knee joint specimens.

Discussion

We have demonstrated that the PM-UTE-AdiabT$_{1\rho}$ sequence allows volumetric $T_{1\rho}$ mapping of both short and long T_2 tissues in the whole knee joint on a clinical 3T scanner. Phantom studies suggest that $T_{1\rho}$ measures provided by the PM-UTE-AdiabT$_{1\rho}$ technique are sensitive to compositional changes and these measurements are reproducible. The ex vivo and in vivo knee studies demonstrate the feasibility of quantifying $T_{1\rho}$ for all the major tissue components in the knee joint including the articular cartilage, meniscus, PCL, ACL, patellar tendon, and muscle.

The 3D MAPSS CW-$T_{1\rho}$ sequence has been widely used to evaluate tissue degeneration and monitor compositional changes longitudinally in the musculoskeletal system [31–36]. Some of the sequence features in 3D MAPSS, such as magnetization reset, phase modulation, and VFA scheme [23], have been successfully incorporated in the PM-UTE-AdiabT$_{1\rho}$ sequence. The successful implementation of these features was validated by the second phantom study, which demonstrated a strong linear correlation ($R^2 = 0.9971$) and a similar value range (i.e., [20, 100] ms) between PM-UTE-CW-$T_{1\rho}$ and MAPSS CW-$T_{1\rho}$ measurements. With these features implemented in PM-UTE-AdiabT$_{1\rho}$, T_1 measurement is no longer needed, and a simple exponential fitting is sufficient for accurate UTE-AdiabT$_{1\rho}$ quantification. In addition, the first phantom study further demonstrates the excellent reproducibility of this framework used in the PM-UTE-AdiabT$_{1\rho}$ sequence.

We have demonstrated in this study that the PM-UTE-AdiabT$_{1\rho}$ sequence is able to quantify all the major tissue components in the knee joint, including both short (e.g., the deep cartilage, menisci, ligaments, and tendons) and long T_2 (e.g., the superficial cartilage, and muscle) tissues. This is because the PM-UTE-AdiabT$_{1\rho}$ sequence uses a very short TE (e.g., 0.032 ms) for data acquisition [25]. Thus the collagen-rich short T_2 tissues can also be imaged and quantified. This allows more comprehensive assessment of musculoskeletal diseases, such as knee OA. Knee OA has been recognized as a whole organ disease [37]. Any tissue deterioration or misalignment in the knee joint can accelerate the progression of OA [38]. Studies also show that meniscal positioning or collateral ligament damage can lead to cartilage loss [39,40]. As such, the developed PM-UTE-AdiabT$_{1\rho}$ sequence provides great potential in studying knee OA comprehensively.

A 3T cartilage study has shown that the 3D MAPSS-$T_{1\rho}$ sequence with a CW type spin-lock scheme is sensitive to the magic angle effect [6]. The CW-$T_{1\rho}$ values are more than

doubled when the tissue fibers reorientate from 0° to 55° relative to the B_0 field [6–8]. Most recently, both ex vivo enzymatic degradation studies and in vivo OA studies have shown that Adiab$T_{1\rho}$ is sensitive to biochemical changes in articular cartilage [13,15,17]. More importantly, Adiab$T_{1\rho}$ is much less sensitive to the magic angle effect than CW-$T_{1\rho}$ as demonstrated in previous cartilage and tendon studies on a clinical 3T MRI [8,9].

In addition to the reduced sensitivity to the magic angle effect, the Adiab$T_{1\rho}$ preparation typically has a lower total RF power deposition than the CW-$T_{1\rho}$ preparation. This is because the AFP pulse employs both amplitude and frequency modulation rather than amplitude only, which is used in CW type preparation for spin locking [11]. The specific absorption rate (SAR) is directly related to the amplitude of the spin locking pulse [41]. Moreover, the PM-UTE-Adiab$T_{1\rho}$ imaging is insensitive to B_1 inhomogeneity because of the adiabatic pulse character [11]. In contrast, the conventional CW-$T_{1\rho}$ imaging suffers from B_1 inhomogeneity related banding artifacts [18–20]. These advantages of Adiab$T_{1\rho}$ preparation will be even more favorable in high field MRI (e.g., 7T) where the SAR issue and B_1 inhomogeneity become more significant.

The contrast mechanism of Adiab$T_{1\rho}$ is still not very well-understood. The spin-lock direction of Adiab$T_{1\rho}$ varies from the z-axis to the x-y plane and then back to the z-axis. In comparison, the spins are only locked in the x-y plane during CW-$T_{1\rho}$ preparation. Dipole-dipole interaction may affect apparent $T_{1\rho}$ more in the x-y plane than in the z-axis, as demonstrated in the orientation sensitivity of T_2 and T_1 relaxation times, respectively [42,43]. This could lead to a shorter $T_{1\rho}$ measured by CW-$T_{1\rho}$ in comparison to Adiab$T_{1\rho}$ when the tissue fiber orientation is parallel to the B_0 field, which means that CW-$T_{1\rho}$ is more sensitive to the magic angle effect [44]. If the spin-lock frequency of CW-$T_{1\rho}$ is sufficiently high (e.g., ≥1 kHz), the effect of dipole-dipole interaction for $T_{1\rho}$ measurement may be negligible compared with the slow-motion interactions between motion-restricted water molecules and their local macromolecular environment [10]. Due to the relatively higher spin-lock frequency of the Adiab$T_{1\rho}$ preparation (from 724 to 860 Hz in this study, calculated by the square root of the real and imaginary parts of the AFP pulses), the measured $T_{1\rho}$ values from the Adiab$T_{1\rho}$ type sequences are generally higher than those measured from the typical CW-$T_{1\rho}$ type sequences (≤500 Hz) on a clinical scanner [10,13,23]. Our measured in vivo cartilage $T_{1\rho}$ value (77.9±3.9 ms) is similar to the reported values (from 69.0 to 79.9 ms) from a recent Adiab$T_{1\rho}$ study [13].

A recent letter article from Pang Y explained how a $T_{1\rho}$ relaxation time measured using Adiab$T_{1\rho}$ preparation was relatively longer than when using a CW-$T_{1\rho}$ preparation [24]. The article claimed that the Adiab$T_{1\rho}$ quantification was subject to T_1 contamination during each relatively long AFP pulse (even for a 2 ms pulse), but there was no validated theory or dedicated experimental data provided in the letter article to support the T_1 contamination assumption. Though our phantom study showed a moderate correlation between PM-UTE-Adiab$T_{1\rho}$ and T_1 measurements (R^2 = 0.3633, P = 0.038), this does not necessarily mean there is T_1 contamination in the Adiab$T_{1\rho}$ measurement given that a similar moderate correlation was also found between MAPSS CW-$T_{1\rho}$ and T_1 measurements (R^2 = 0.3846, P = 0.031), and the MAPSS CW-$T_{1\rho}$ measurement is T_1-independent in theory. More interestingly, the $T_{1\rho}$ values measured by the proposed PM-UTE-Adiab$T_{1\rho}$

linearly correlated with the MAPSS CW-$T_{1\rho}$ measurements ($R^2 = 0.9985$, $P < 0.0001$). This strong correlation demonstrates that the PM-UTE-Adiab$T_{1\rho}$ measurements may be also unaffected by T_1 contamination, considering that the MAPSS CW-$T_{1\rho}$ measurement is theoretically T_1-independent. Moreover, the strong linear correlation also demonstrates the comparable sensitivity between PM-UTE-Adiab$T_{1\rho}$ and MAPSS CW-$T_{1\rho}$ techniques in detecting compositional changes. We believe that one of the major contributing factors for the higher Adiab$T_{1\rho}$ values is the higher spin-lock frequencies used in the Adiab$T_{1\rho}$ preparation compared to the CW-$T_{1\rho}$ preparation on a clinical scanner, which was not mentioned in Pang Y's letter article. Indeed, more research is needed to better understand the mechanism of Adiab$T_{1\rho}$ relaxation.

To further investigate the contrast mechanism of both Adiab$T_{1\rho}$ and CW-$T_{1\rho}$, we plan to perform a comparison study (i.e., PM-UTE-Adiab$T_{1\rho}$ vs. PM-UTE-CW$T_{1\rho}$) on a newly installed small-bore Bruker 3T scanner. In addition to the state-of-art preparation scheme for CW-$T_{1\rho}$, a few new CW-$T_{1\rho}$ developments will also be incorporated with the PM-UTE sequence structure in this comparison study [45]. Typically, the maximum spin-lock frequency of CW-$T_{1\rho}$ is limited by the peak power of the RF amplifier and SAR restriction on a clinical 3T scanner. The Bruker scanner offers more flexibility in adjusting the spin-lock frequencies than the clinical 3T scanner used in this study, thus providing more useful information in studying the mechanisms of CW-$T_{1\rho}$ and Adiab$T_{1\rho}$. Magic angle effects will also be investigated on different spin-lock frequencies as well.

This study has several limitations. First, the total number of ex vivo and in vivo knee joints is relatively small, which is justified for this technical evaluation study. Second, we have only demonstrated the technical feasibility of the 3D PM-UTE-Adiab$T_{1\rho}$ sequence for volumetric $T_{1\rho}$ mapping of both short and long T_2 tissues in normal knee joints of healthy volunteers. Patients with knee OA are not recruited for this study. The ex vivo knee joints also have relatively normal morphology. Histology was not performed to confirm the degeneration status in each knee joint specimen. Third, although the new sequence eliminates the need for T_1 measurement, it comes at the cost of prolonged scan time since two acquisitions with the same gradient encodings must be scanned. The scan time can be reduced with a smaller number of TSLs, longer spiral interleaves for data acquisition, and more spokes (i.e., a higher N_{sp} value) in each TR [46,47]. Moreover, fast imaging techniques such as compressed sensing or deep learning can be incorporated to further accelerate data acquisition [48–51]. Fourth, the image signal-to-noise ratio increases when a longer T_{rec} is used, leading to a longer total scan time. Longer T_{rec}s will be investigated when fast imaging techniques are available to accelerate the PM-UTE-Adiab$T_{1\rho}$ scan.

Conclusion

The newly proposed PM-UTE-Adiab$T_{1\rho}$ sequence allows comprehensive quantification of all the major tissue components in the knee joint, demonstrating its potential in future clinical studies of knee OA.

Supplementary Material

Refer to Web version on PubMed Central for supplementary material.

Acknowledgments

The authors acknowledge grant support from the National Institutes of Health (R01AR062581, R01AR068987, R01AR075825, R01AR078877, R01AR079484, P30AR073761, and R21AR075851), the VA Clinical Science Research & Development Service (I01CX001388, and I01CX000625), and GE Healthcare.

References

1. Wang L, Regatte RR. T1ρ MR Imaging of Human Musculoskeletal System. J Magn Reson Imaging. 2015;41(3):586–600. doi:10.1002/jmri.24677 [PubMed: 24935818]
2. Duvvuri U, Reddy R, Patel SD, Kaufman JH, Kneeland JB, Leigh JS. T1rho-relaxation in articular cartilage: effects of enzymatic degradation. Magn Reson Med. 1997;38:863–867. [PubMed: 9402184]
3. Regatte RR, Akella SVS, Lonner JH, Kneeland JB, Reddy R. T1rho relaxation mapping in human osteoarthritis (OA) cartilage: comparison of T1rho with T2. J Magn Reson Imaging. 2006;23:547–553. [PubMed: 16523468]
4. Li X, Han ET, Ma CB, Link TM, Newitt DC, Majumdar S. In vivo 3T spiral imaging based multi-slice T1ρ mapping of knee cartilage in osteoarthritis. Magnetic Resonance in Medicine: An Official Journal of the International Society for Magnetic Resonance in Medicine. 2005;54(4):929–936.
5. Wang N, Xia Y. Dependencies of multi-component T2 and T1ρ relaxation on the anisotropy of collagen fibrils in bovine nasal cartilage. Journal of magnetic Resonance. 2011;212(1):124–132. [PubMed: 21788148]
6. Shao H, Pauli C, Li S, et al. Magic angle effect plays a major role in both T1rho and T2 relaxation in articular cartilage. Osteoarthritis Cartilage. 2017;25:2022–2030. [PubMed: 28161394]
7. Du J, Statum S, Znamirowski R, Bydder GM, Chung CB. Ultrashort TE T1ρ magic angle imaging. Magn Reson Med. 2013;69(3):682–687. doi:10.1002/mrm.24296 [PubMed: 22539354]
8. Wu M, Ma Y, Wan L, et al. Magic angle effect on adiabatic T1rho imaging of the Achilles tendon using 3D ultrashort echo time cones trajectory. NMR Biomed. 2020;33:e4322. [PubMed: 32431025]
9. Wu M, Ma Y, Kasibhatla A, et al. Convincing evidence for magic angle less-sensitive quantitative T1rho imaging of articular cartilage using the 3D ultrashort echo time cones adiabatic T1rho (3D UTE Cones-AdiabT1rho) sequence. Magn Reson Med. 2020;84:2551–2560. [PubMed: 32419199]
10. Hänninen N, Rautiainen J, Rieppo L, Saarakkala S, Nissi MJ. Orientation anisotropy of quantitative MRI relaxation parameters in ordered tissue. Sci Rep. 2017;7:9606. [PubMed: 28852032]
11. Garwood M, DelaBarre L. The return of the frequency sweep: designing adiabatic pulses for contemporary NMR. Journal of magnetic resonance. 2001;153(2):155–177. [PubMed: 11740891]
12. Michaeli S, Sorce DJ, Springer CS Jr, Ugurbil K, Garwood M. T1ρ MRI contrast in the human brain: modulation of the longitudinal rotating frame relaxation shutter-speed during an adiabatic RF pulse. Journal of magnetic resonance. 2006;181(1):135–147. [PubMed: 16675277]
13. Casula V, Autio J, Nissi MJ, et al. Validation and optimization of adiabatic T1ρ and T2ρ for quantitative imaging of articular cartilage at 3 T. Magnetic resonance in medicine. 2017;77(3):1265–1275. [PubMed: 26946182]
14. Zhang J, Nissi M j., Idiyatullin D, Michaeli S, Garwood M, Ellermann J. Capturing fast relaxing spins with SWIFT adiabatic rotating frame spin–lattice relaxation (T1ρ) mapping. NMR in Biomedicine. 2016;29(4):420–430. doi:10.1002/nbm.3474 [PubMed: 26811973]
15. Rautiainen J, Nissi MJ, Salo EN, et al. Multiparametric MRI assessment of human articular cartilage degeneration: Correlation with quantitative histology and mechanical properties. Magnetic Resonance in Medicine. 2015;74(1):249–259. doi:10.1002/mrm.25401 [PubMed: 25104181]

16. Jerban S, Ma Y, Kasibhatla A, et al. Ultrashort echo time adiabatic T1ρ (UTE-Adiab-T1ρ) is sensitive to human cadaveric knee joint deformation induced by mechanical loading and unloading. Magnetic Resonance Imaging. 2021;80:98–105. doi:10.1016/j.mri.2021.04.014 [PubMed: 33945858]
17. Wu M, Ma YJ, Liu M, et al. Quantitative assessment of articular cartilage degeneration using 3D ultrashort echo time cones adiabatic T1ρ (3D UTE-Cones-AdiabT1ρ) imaging. Eur Radiol. 2022;32(9):6178–6186. doi:10.1007/s00330-022-08722-6 [PubMed: 35357540]
18. Chen W Artifacts correction for T1rho imaging with constant amplitude spin-lock. J Magn Reson. 2017;274:13–23. doi:10.1016/j.jmr.2016.11.002 [PubMed: 27842257]
19. Chen W Errors in quantitative T1rho imaging and the correction methods. Quantitative Imaging in Medicine and Surgery. 2015;5(4):58391–58591. doi:10.3978/j.issn.2223-4292.2015.08.05
20. Witschey WRT, Borthakur A, Elliott MA, et al. Artifacts in T1ρ-Weighted Imaging: Compensation for B1 and B0 Field Imperfections. J Magn Reson. 2007;186(1):75–85. doi:10.1016/j.jmr.2007.01.015 [PubMed: 17291799]
21. Ma Y, Carl M, Searleman A, Lu X, Chang EY, Du J. 3D Adiabatic T1rho prepared Ultrashort Echo Time Cones (3D AdiabT1rho UTE-Cones) sequence for whole knee imaging. Magn Reson Med. 2018;80:1429–1439. [PubMed: 29493004]
22. Wu M, Zhao W, Wan L, et al. Quantitative three-dimensional ultrashort echo time cones imaging of the knee joint with motion correction. NMR in Biomedicine. 2020;Jan;33(1):e4214. [PubMed: 31713936]
23. Li X, Han ET, Busse RF, Majumdar S. In vivo T(1rho) mapping in cartilage using 3D magnetization-prepared angle-modulated partitioned k-space spoiled gradient echo snapshots (3D MAPSS). Magn Reson Med. 2008;59(2):298–307. doi:10.1002/mrm.21414 [PubMed: 18228578]
24. Pang Y An adiabatic RF pulse in spin-lock preparations: A double-edged sword for quantitative R1ρ imaging in clinical applications. NMR in Biomedicine. 2023:e4953.
25. Carl M, Bydder GM, Du J. UTE imaging with simultaneous water and fat signal suppression using a time-efficient multispoke inversion recovery pulse sequence. Magnetic Resonance in Medicine. 2016;76(2):577–582. doi:10.1002/mrm.25823 [PubMed: 26309221]
26. Ma Y, Zhu Y, Lu X, Carl M, Chang EY, Du J. Short T2 Imaging Using a Three-Dimensional Double Adiabatic Inversion Recovery Prepared Ultrashort Echo Time Cones (3D DIR-UTE-Cones) Sequence. Magn Reson Med. 2018;79:2555–2563. [PubMed: 28913879]
27. Ma YJ, Chen Y, Li L, et al. Trabecular bone imaging using a 3D adiabatic inversion recovery prepared ultrashort TE Cones sequence at 3T. Magnetic Resonance in Medicine. 2020;83(5):1640–1651. [PubMed: 31631404]
28. Ma YJ, Zhao W, Wan L, et al. Whole knee joint T1 values measured in vivo at 3T by combined 3D ultrashort echo time cones actual flip angle and variable flip angle methods. Magnetic resonance in medicine. 2019;81(3):1634–1644. [PubMed: 30443925]
29. Levenberg K A method for the solution of certain non-linear problems in least squares. Quarterly of applied mathematics. 1944;2(2):164–168.
30. Marquardt DW. An algorithm for least-squares estimation of nonlinear parameters. Journal of the society for Industrial and Applied Mathematics. 1963;11(2):431–441.
31. Chen E, Amano K, Pedoia V, Souza RB, Ma CB, Li X. Longitudinal analysis of tibiofemoral cartilage contact area and position in ACL reconstructed patients. Journal of Orthopaedic Research. 2018;36(10):2718–2727. doi:10.1002/jor.24024 [PubMed: 29667733]
32. Mamoto K, Xu K, Shimizu T, et al. T1ρ and T2 of articular cartilage after acl injury predict patient-reported outcomes at 3 years after acl reconstruction. Osteoarthritis and Cartilage. 2018;26:S49–S50. doi:10.1016/j.joca.2018.02.113
33. Blumenkrantz G, Zuo J, Li X, Kornak J, Link TM, Majumdar S. In vivo 3.0-tesla magnetic resonance T1rho and T2 relaxation mapping in subjects with intervertebral disc degeneration and clinical symptoms. Magn Reson Med. 2010;63(5):1193–1200. doi:10.1002/mrm.22362 [PubMed: 20432290]
34. Roach KE, Souza RB, Majumdar S, Pedoia V. Local Patterns in 2-Year T1ρ and T2 Changes of Hip Cartilage Are Related to Sex and Functional Data: A Prospective Evaluation on Hip Osteoarthritis Participants. J Magn Reson Imaging. July 2022. doi:10.1002/jmri.28347

35. Rauscher I, Stahl R, Cheng J, et al. Meniscal measurements of T1rho and T2 at MR imaging in healthy subjects and patients with osteoarthritis. Radiology. 2008;249(2):591–600. [PubMed: 18936315]
36. Xie D, Murray J, Lartey R, et al. Multi-vendor multi-site quantitative MRI analysis of cartilage degeneration 10 Years after anterior cruciate ligament reconstruction: MOON-MRI protocol and preliminary results. Osteoarthritis and Cartilage. 2022;30(12):1647–1657. [PubMed: 36049665]
37. Brandt KD, Radin EL, Dieppe PA, Van De Putte L. Yet more evidence that osteoarthritis is not a cartilage disease. Annals of the rheumatic diseases. 2006;65(10):1261–1264. [PubMed: 16973787]
38. Hunter DJ, Zhang Y, Niu J, et al. Structural factors associated with malalignment in knee osteoarthritis: the Boston osteoarthritis knee study. The Journal of rheumatology. 2005;32(11):2192–2199. [PubMed: 16265702]
39. Hunter DJ, Zhang YQ, Niu JB, et al. The association of meniscal pathologic changes with cartilage loss in symptomatic knee osteoarthritis. Arthritis & Rheumatism. 2006;54(3):795–801. [PubMed: 16508930]
40. Tan AL, Toumi H, Benjamin M, et al. Combined high-resolution magnetic resonance imaging and histological examination to explore the role of ligaments and tendons in the phenotypic expression of early hand osteoarthritis. Annals of the rheumatic diseases. 2006;65(10):1267–1272. [PubMed: 16627540]
41. Wheaton AJ, Borthakur A, Corbo M, Charagundla SR, Reddy R. Method for reduced SAR T1ρ-weighted MRI. Magnetic Resonance in Medicine. 2004;51(6):1096–1102. doi:10.1002/mrm.20141 [PubMed: 15170827]
42. Xia Y Relaxation anisotropy in cartilage by NMR microscopy (muMRI) at 14-microm resolution. Magn Reson Med. 1998;39(6):941–949. doi:10.1002/mrm.1910390612 [PubMed: 9621918]
43. Xia Y, Moody JB, Alhadlaq H. Orientational dependence of T2 relaxation in articular cartilage: A microscopic MRI (microMRI) study. Magn Reson Med. 2002;48(3):460–469. [PubMed: 12210910]
44. Mlynárik V, Szomolányi P, Toffanin R, Vittur F, Trattnig S. Transverse relaxation mechanisms in articular cartilage. J Magn Reson. 2004;169(2):300–307. [PubMed: 15261626]
45. Pala S, Hänninen NE, Nykänen O, Liimatainen T, Nissi MJ. New methods for robust continuous wave T1ρ relaxation preparation. NMR Biomed. 2023;36(2):e4834. [PubMed: 36115012]
46. Wan L, Zhao W, Ma Y, et al. Fast quantitative 3D ultrashort echo time MRI of cortical bone using extended cones sampling. Magnetic Resonance in Medicine. 2019;82(1):225–236. [PubMed: 30821032]
47. Wan L, Ma Y, Yang J, et al. Fast quantitative three-dimensional ultrashort echo time (UTE) Cones magnetic resonance imaging of major tissues in the knee joint using extended sprial sampling. NMR in Biomedicine. 2020;33(10):e4376. doi:10.1002/nbm.4376 [PubMed: 32667115]
48. Athertya JS, Ma Y, Masoud Afsahi A, et al. Accelerated Quantitative 3D UTE-Cones Imaging Using Compressed Sensing. Sensors. 2022;22(19):7459. doi:10.3390/s22197459 [PubMed: 36236557]
49. Ma YJ, Searleman AC, Jang H, et al. Whole-Brain Myelin Imaging Using 3D Double-Echo Sliding Inversion Recovery Ultrashort Echo Time (DESIRE-UTE) MRI. Radiology. 2020;294(2):362–374. [PubMed: 31746689]
50. Wu Y, Ma Y, Liu J, Du J, Xing L. Self-attention convolutional neural network for improved MR image reconstruction. Information Sciences. 2019;490:317–328. [PubMed: 32817993]
51. Wu Y, Ma Y, Capaldi DP, et al. Incorporating prior knowledge via volumetric deep residual network to optimize the reconstruction of sparsely sampled MRI. Magnetic Resonance Imaging. 2020;66:93–103. doi:10.1016/j.mri.2019.03.012 [PubMed: 30880112]

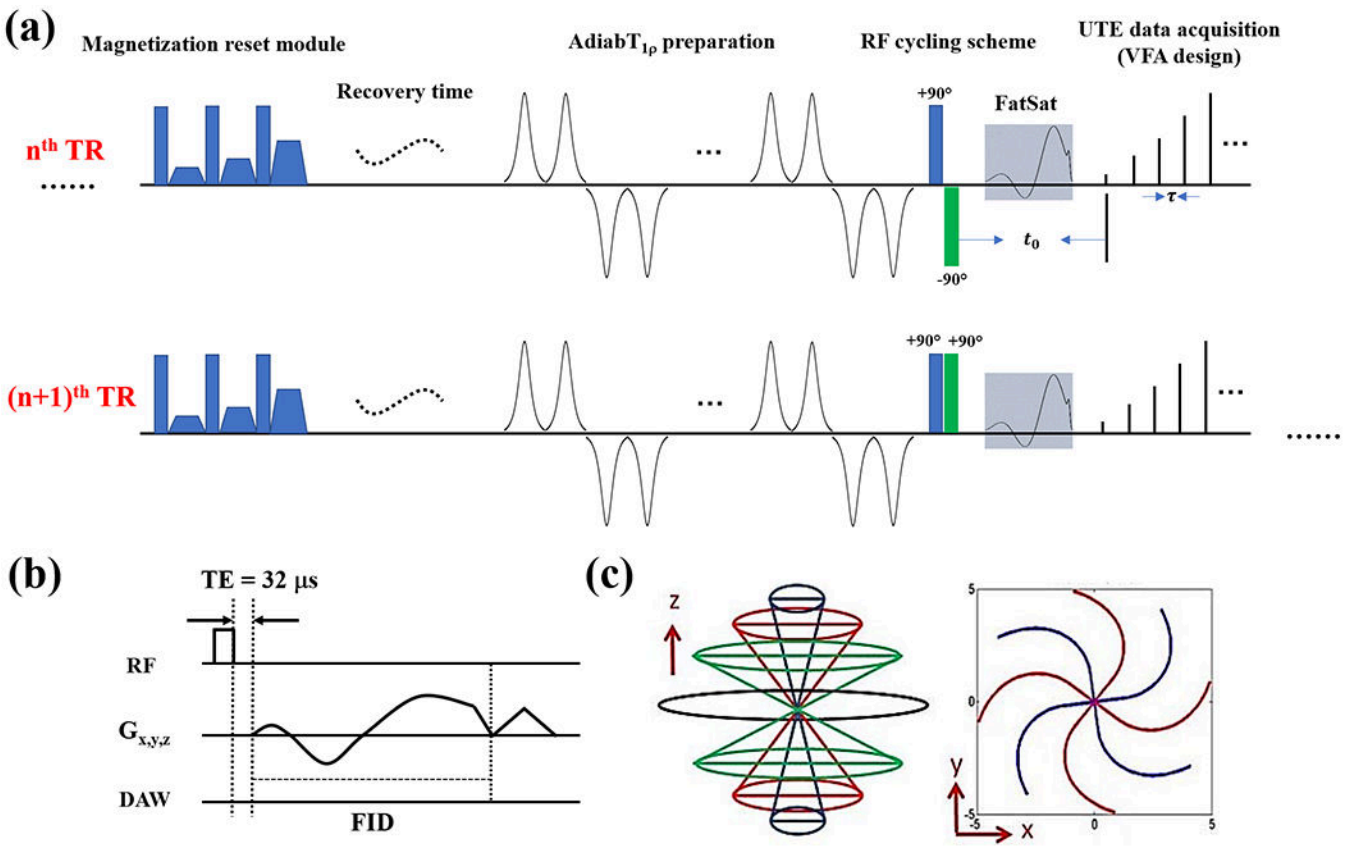

Figure 1.

Diagram of the PM-UTE-Adiab$T_{1\rho}$ sequence. This new sequence includes six major features: 1) a magnetization reset module (**a**), 2) an Adiab$T_{1\rho}$ preparation using a train of AFP pulses for spin locking (**a**), 3) a phase modulation scheme (i.e., RF cycling scheme using a 90° pulse pair) (**a**), 4) a fat saturation module (**a**), 5) a VFA excitation scheme (**a**), and 6) a 3D UTE sequence for data acquisition (**b**). The adjacent two acquisitions (e.g., for n^{th} and $(n+1)^{th}$ TRs) have identical parameters except for the RF cycling module (**a**). During the second acquisition, the phase of the second 90° pulse in the RF cycling pair alternates 180°. A rectangular pulse (i.e., 270 μs) is used for signal excitation and the minimal nominal TE (defined as the gap between the excitation pulse and data acquisition window) of this sequence is 32 μs (**b**). An efficient 3D Cones trajectory is utilized for k-space encoding (**c**).

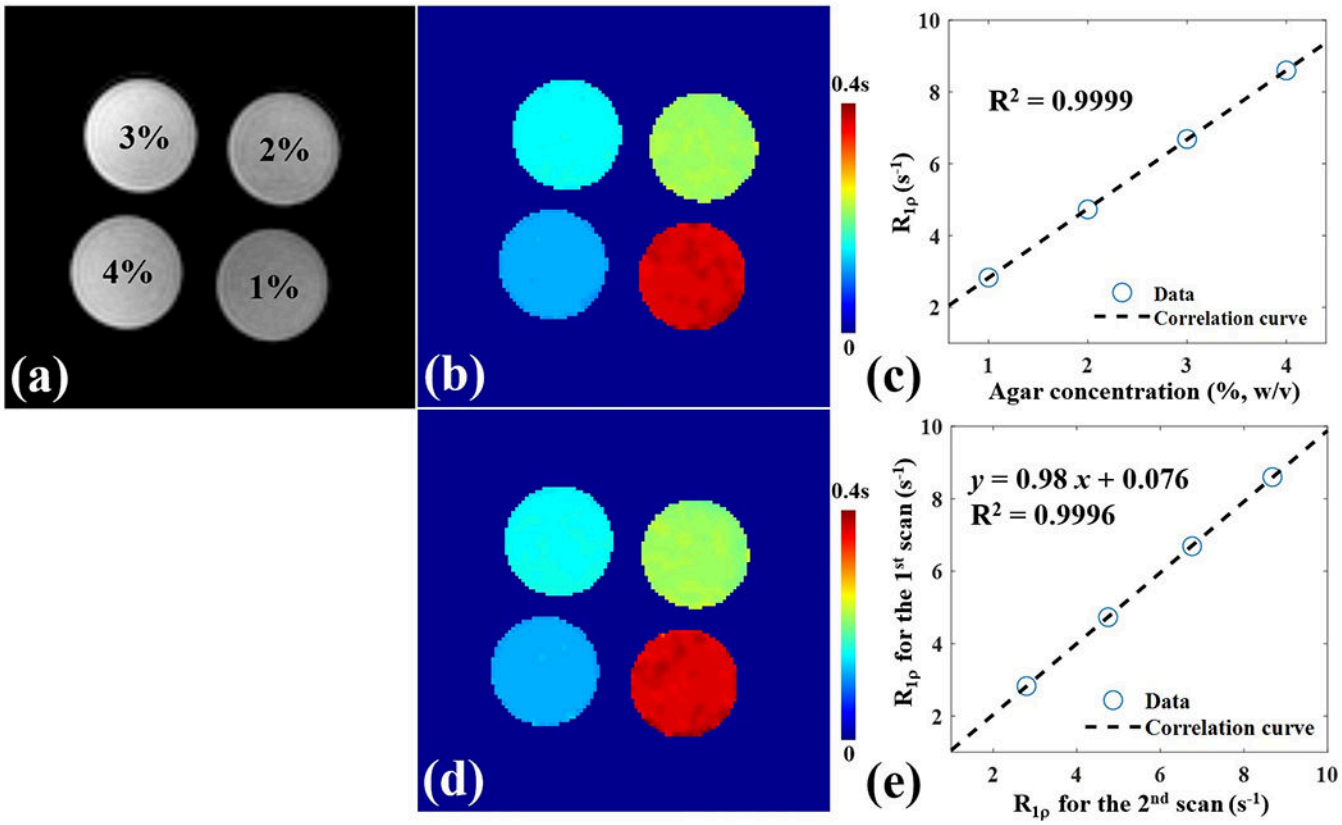

Figure 2.

Phantom imaging results for the studies of tissue compositional sensitivity and scan reproducibility using the PM-UTE-AdiabT$_{1\rho}$ sequence. Phantoms with four different agarose concentrations (i.e., 1, 2, 3, and 4%, w/v) (**a**) are imaged twice and the corresponding T$_{1\rho}$ maps are seen in (**b**) and (**d**). The R$_{1\rho}$ values show excellent linear correlation with agarose concentration with an R^2 of 0.9999 (**c**). Excellent reproducibility of the R$_{1\rho}$ measurement is achieved between the 1st and 2nd scans with an R^2 of 0.9996 (**e**).

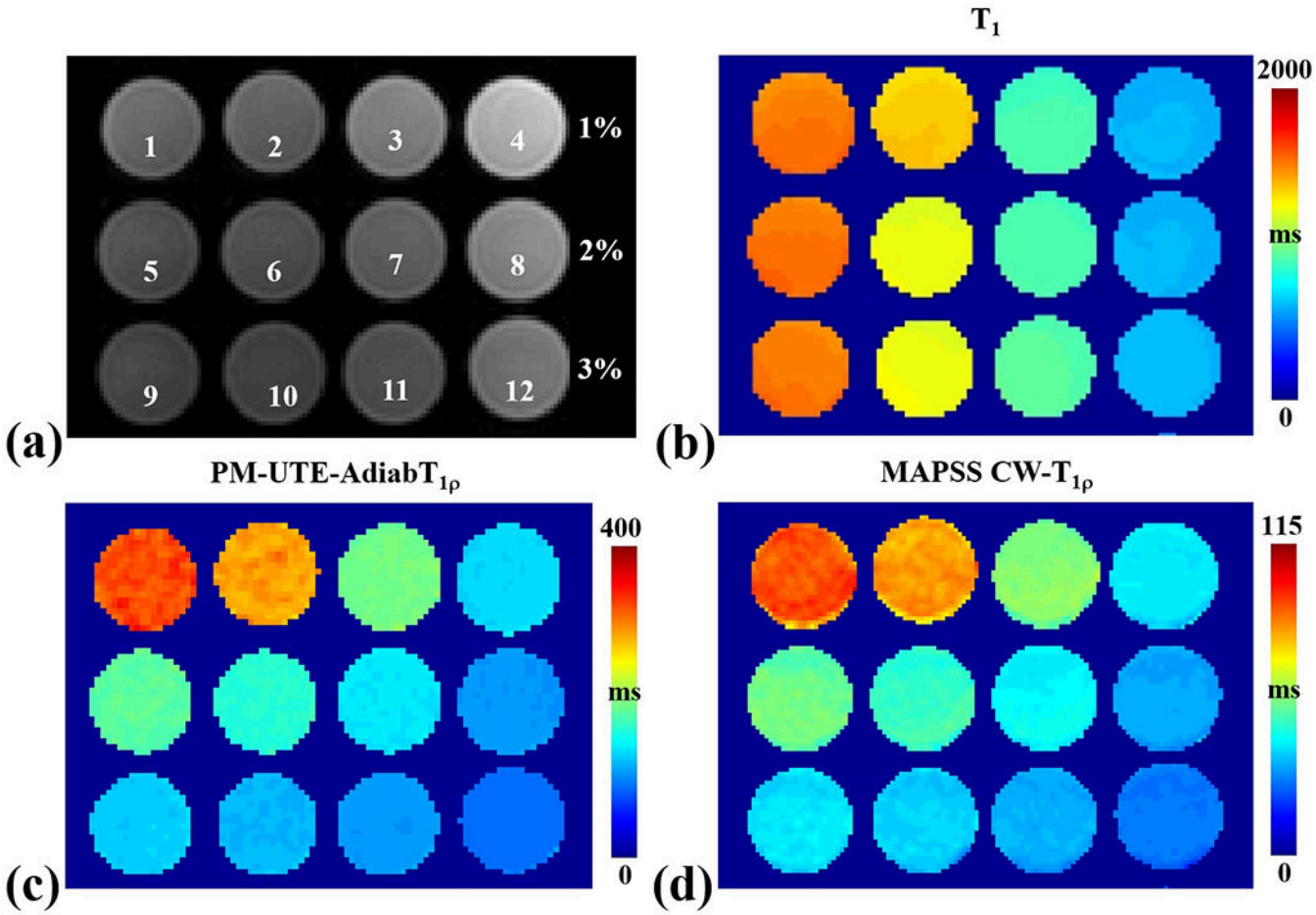

Figure 3.

Phantom imaging results using T_1, PM-UTE-Adiab$T_{1\rho}$, and MAPSS CW-$T_{1\rho}$ mapping techniques. The agarose concentrations are 1%, 2%, and 3% w/v for the twelve phantoms listed in the first (1-4), second (5-8), and third (9-12) rows, respectively (**a**). The quantitative T_1, PM-UTE-Adiab$T_{1\rho}$, and MAPSS CW-$T_{1\rho}$ maps are shown in panels (**b**), (**c**), and (**d**), respectively.

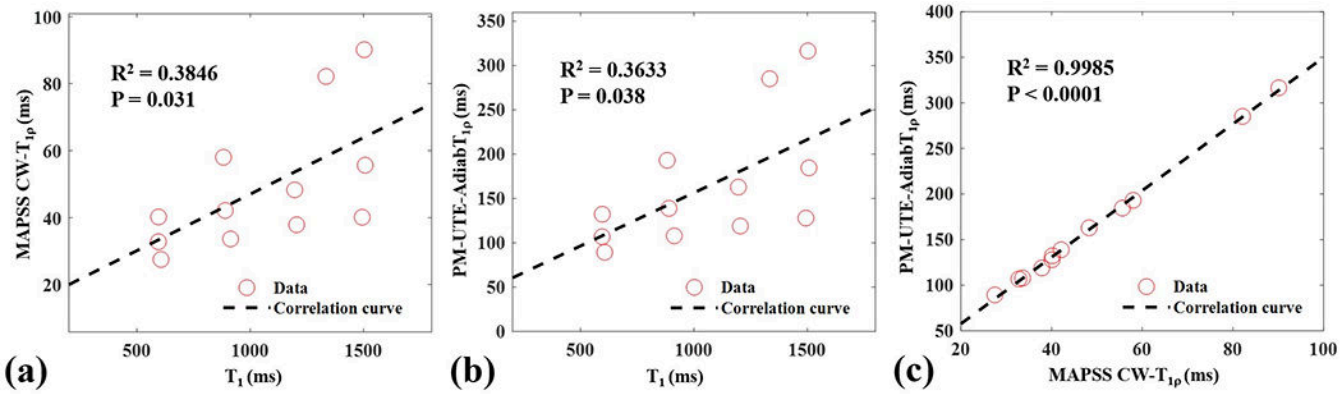

Figure 4.

Correlation curves for the measurements between MAPSS CW-$T_{1\rho}$, PM-UTE-Adiab$T_{1\rho}$, and T_1, and between PM-UTE-Adiab$T_{1\rho}$ and MAPSS CW-$T_{1\rho}$ for the twelve phantoms. A similar moderate correlation is found between MAPSS CW-$T_{1\rho}$ measures and T_1 values (R^2 = 0.3846, P = 0.031) (**a**) and between PM-UTE-Adiab$T_{1\rho}$ measures and T_1 values (R^2 = 0.3633, P = 0.038) (**b**), while a very strong correlation is found between PM-UTE-Adiab$T_{1\rho}$ and MAPSS CW-$T_{1\rho}$ measures (R^2 = 0.9985, P < 0.0001) (**c**).

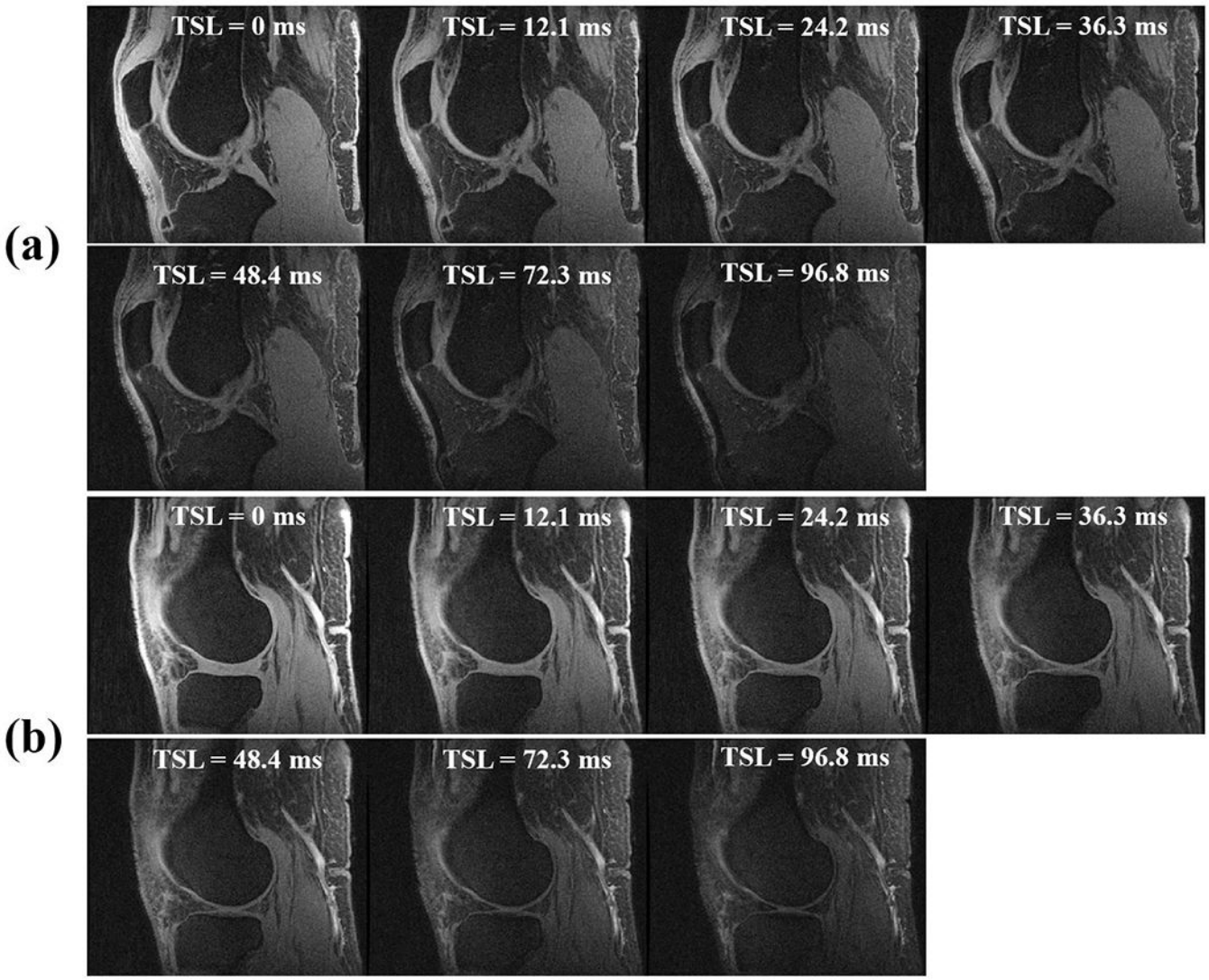

Figure 5.

Representative PM-UTE-Adiab$T_{1\rho}$ images of two different slices (**a** and **b**) from a normal knee specimen (45-year-old male donor) with TSLs ranging from 0 to 96.87 ms. Both short and long T_2 tissue signals are detected by this new sequence. Short T_2 tissue signals decrease faster with increased TSLs. Fat is efficiently suppressed in all images.

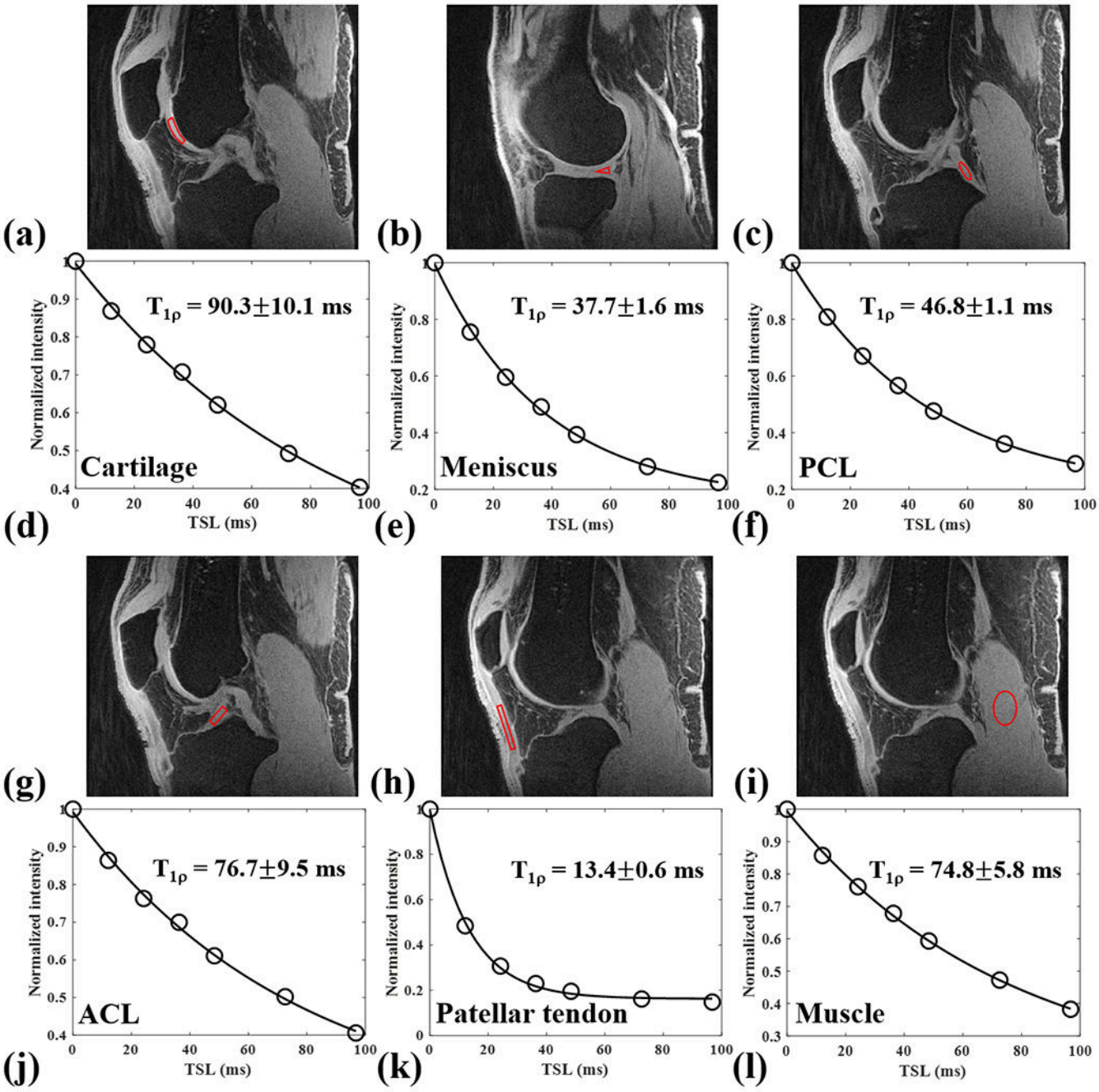

Figure 6.

The PM-UTE-Adiab$T_{1\rho}$ imaging results of the normal knee specimen from the 45-year-old male donor. The fitting curves and corresponding $T_{1\rho}$ values of the femoral cartilage (**a**), meniscus (**b**), PCL (**c**), ACL (**g**), patellar tendon (**h**), and muscle (**i**) (tissue ROIs shown inside of the red closed curves) are 90.3±10.1 ms (**d**), 37.7±1.6 ms (**e**), 46.8±1.1 ms (**f**), 76.7±9.5 ms (**j**), 13.4±0.6 (**k**), and 74.8±5.8 ms (**l**), respectively.

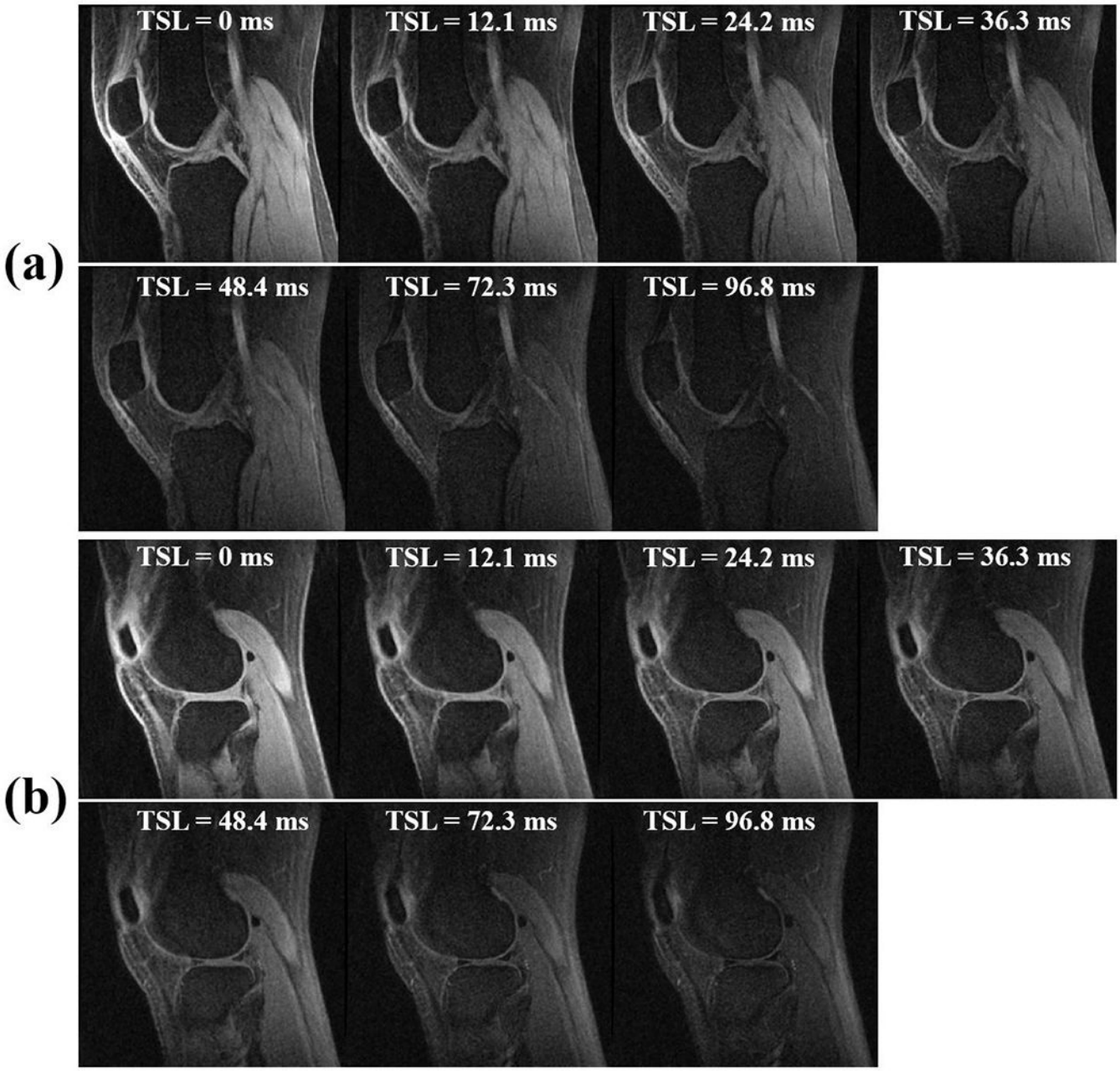

Figure 7.

Representative PM-UTE-Adiab$T_{1\rho}$ images of two different slices (**a** and **b**) from a normal knee joint (36-year-old female volunteer). Both short and long T_2 tissue signals are detected by this new sequence. Signals for short T_2 tissues (e.g., the meniscus and patellar tendon) decrease faster with longer TSLs. Fat is efficiently suppressed in all images.

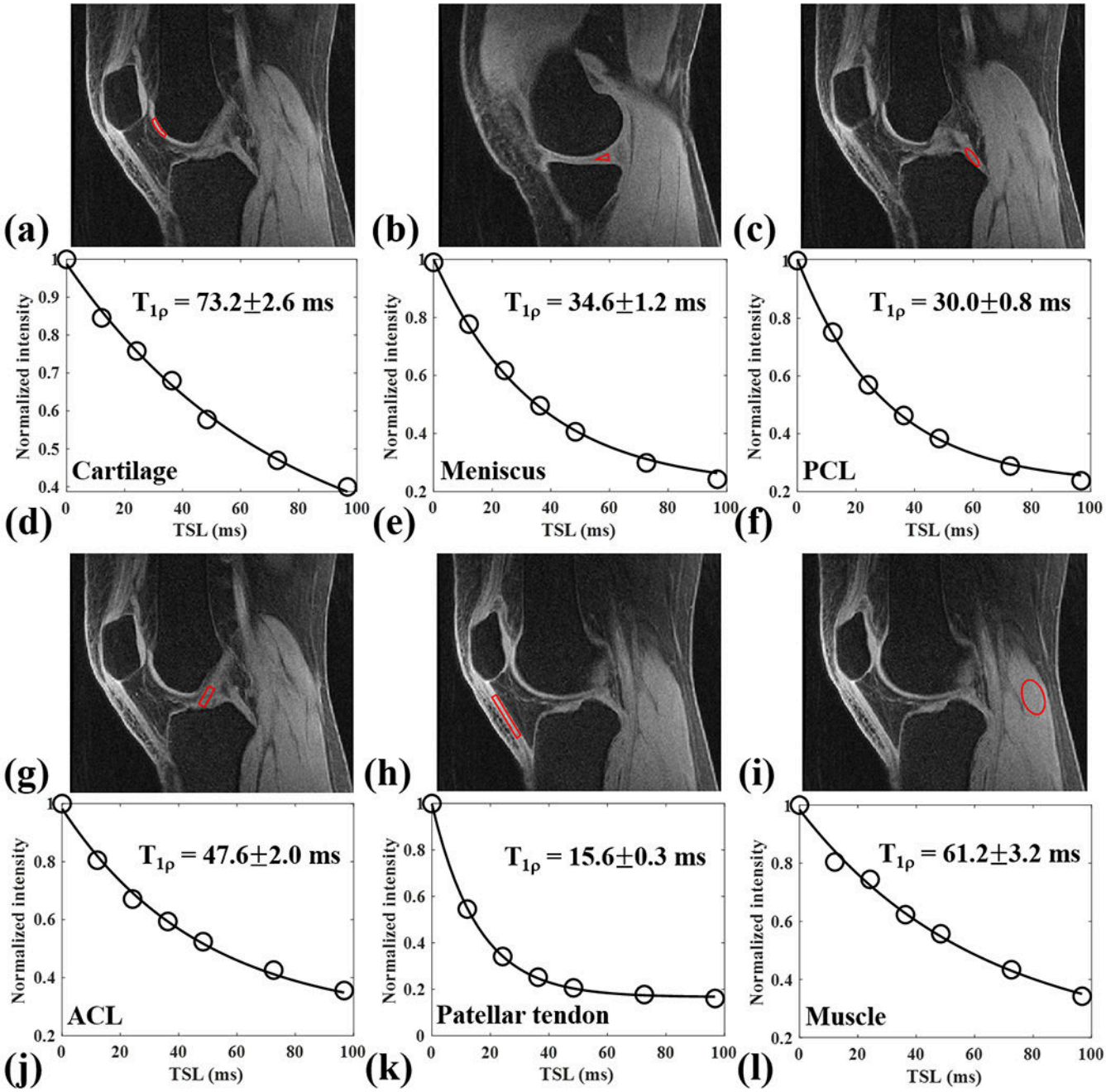

Figure 8.

The PM-UTE-Adiab$T_{1\rho}$ imaging results of the normal knee joint from the 36-year-old female volunteer. The fitting curves and corresponding $T_{1\rho}$ values of the femoral cartilage (**a**), meniscus (**b**), PCL (**c**), ACL (**g**), patellar tendon (**h**), and muscle (**i**) (tissue ROIs shown inside of the red closed curves) are 73.2±2.6 ms (**d**), 34.6±1.2 ms (**e**), 30.0±0.8 ms (**f**), 47.6±2.0 ms (**j**), 15.6±0.3 ms (**k**), and 61.2±3.2 ms (**l**), respectively.

Table 1.

Agarose and $MnCl_2$ concentrations as well as quantitative T_1 values for twelve phantoms (see Figure 3a).

Phantom ID	**#1**	**#2**	**#3**	**#4**	**#5**	**#6**	**#7**	**#8**	**#9**	**#10**	**#11**	**#12**
Agarose concentration (w/v)	1%	1%	1%	1%	2%	2%	2%	2%	3%	3%	3%	3%
$MnCl_2$ concentration (mM)	0.019	0.039	0.071	0.136	0.017	0.034	0.062	0.118	0.015	0.030	0.056	0.106
T_1 (ms)	1503±7.7	1334±7.3	882±3.1	596±1.3	1507±6.2	1196±3.9	890±1.9	595±0.8	1494±6.0	1205±3.9	913±2.6	606±1.3

Table 2.

$T_{1\rho}$ and its fitting standard errors of cartilage, meniscus, PCL, ACL, patellar tendon and muscle in five ex vivo and five in vivo normal knee joints as well as the summarized mean and STD values for each tissue.

$T_{1\rho}$ (ms)		Cartilage	Meniscus	PCL	ACL	Patellar tendon	Muscle
Ex vivo	#1	90.3±10.1	37.7±1.6	46.8±1.1	76.7±9.5	13.4±0.6	74.8±5.8
	#2	112.7±11.3	46.1±0.3	59.4±0.8	87.4±5.3	21.5±2.3	95.3±1.1
	#3	105.4±8.4	31.8±0.8	44.5±0.4	92.0±4.6	17.2±0.9	97.3±1.2
	#4	113.9±8.8	36.7±1.5	52.9±1.6	71.8±1.8	26.9±0.5	89.1±4.2
	#5	105.5±11.6	43.5±2.0	54.2±2.4	67.2±7.9	19.9±2.5	99.2±12.7
	mean±STD	105.6±8.4	39.2±5.1	51.6±5.3	79.0±9.3	19.8±4.5	91.1±8.8
In vivo	#1	73.2±2.6	34.6±1.2	30.0±0.8	47.6±2.0	15.6±0.3	61.2±3.2
	#2	76.2±1.9	30.7±0.9	33.1±1.0	56.5±3.9	16.4±0.5	58.7±1.7
	#3	76.3±2.6	29.5±0.4	28.8±0.4	54.1±2.4	17.1±0.5	52.8±0.7
	#4	79.0±3.6	28.3±0.7	25.6±1.7	50.0±3.8	15.7±0.3	57.2±2.9
	#5	84.8±2.9	31.8±1.0	28.3±0.3	52.0±1.4	20.4±0.8	58.3±1.8
	mean±STD	77.9±3.9	30.1±2.2	29.2±2.4	52.0±3.1	17.0±1.8	57.6±2.8